Red Sm:KGd(WO_4)_2 laser at 649 nm

Amandine Baillard, Pavel Loiko, Daniel Rytz, Sebastian Schwung, Michaël Fromager, Alain Braud, Patrice Camy

Red Sm:KGd(WO$_4$)$_2$ laser at 649 nm

Amandine Baillard,[1] Pavel Loiko,[1] Daniel Rytz,[2] Sebastian Schwung,[2] Michaël Fromager,[1] Alain Braud,[1] and Patrice Camy[1,*]

[1]*Centre de Recherche sur les Ions, les Matériaux et la Photonique (CIMAP), UMR 6252 CEA-CNRS-ENSICAEN, Université de Caen Normandie, 6 Boulevard Maréchal Juin, 14050 Caen Cedex 4, France*
[2]*EOT GmbH, Struthstraße 2, D-55743, Idar-Oberstein, Germany*
**Corresponding author: patrice.camy@ensicaen.fr*

Received XX Month XXXX; revised XX Month, XXXX; accepted XX Month XXXX; posted XX Month XXXX (Doc. ID XXXXX); published XX Month XXXX

We report on the first laser operation of a Sm^{3+}-doped monoclinic KGd(WO$_4$)$_2$ double tungstate crystal in the red spectral range. Pumped by a frequency-doubled Optically Pumped Semiconductor Laser (2ω-OPSL) at 479.1 nm, the 0.8 at.% Sm:KGd(WO$_4$)$_2$ laser generated an output power up to 17.6 mW at 649.1 nm (the $^4G_{5/2} \rightarrow {}^6H_{9/2}$ transition) with a slope efficiency of 16.9%, a laser threshold down to 29 mW and a linear polarization. The laser exhibited a self-pulsing behavior delivering μs-long pulses with a repetition rate of a few kHz. The polarized spectroscopic properties of Sm^{3+} ions were determined as well. © 2023 Optical Society of America

http://dx.doi.org/10.1364/OL.99.099999

Trivalent samarium ions (Sm^{3+}) possess an electronic configuration of [Xe]4f^5 with a group of lower-lying multiplets ^6F_J and ^6H_J ($^6H_{5/2}$ is the ground-state), and a metastable state $^4G_{5/2}$ exhibiting a relatively long luminescence lifetime (in the ms range). This energy-level structure gives rise to multiple emissions in the visible and near-IR out of which the most prominent ones fall into orange (605 nm, $^4G_{5/2} \rightarrow {}^6H_{7/2}$) and red (650 nm, $^4G_{5/2} \rightarrow {}^6H_{9/2}$) spectral ranges [1]. Nowadays, Sm^{3+}-based phosphors are used in white LEDs and in medical imaging for dosimeter applications [2].

Sm^{3+} ions appear attractive for the development of laser sources directly emitting orange and red radiation. In particular, red lasers find applications in medicine (in dentistry, in Laser Speckle Contrast Imaging to visualize the blood flow, and in oximetry to measure the oxygen content in the blood) [3], as well as in scanning fluorescence microscopy for biochemistry [4].

The development of Sm^{3+} laser was stimulated by the progress in pump sources addressing the blue spectral range, i.e., InGaAs-based frequency-doubled Optically Pumped Semiconductor Lasers (2ω-OPSL) and blue InGaN-based laser diodes [1]. In particular, Sm^{3+} ions feature high absorption in the blue, at 405 nm, due to the $^6H_{5/2} \rightarrow {}^6P_{3/2}$ spin-allowed ($\Delta S = 0$) transition.

The first laser action with Sm^{3+} ions was obtained in 1979 in a 0.1 at.% Sm:TbF$_3$ crystal at cryogenic (116 K) temperature under Xe flash lamp pumping (Tb^{3+} ions enhanced the pump absorption) [5]. Farries *et al.* used a Sm^{3+}-doped silica glass fiber pumped by an Ar$^+$ ions laser (488 nm) to generate 28 mW of continuous-wave (CW) output at 651 nm with a laser threshold of ~20 mW [6]. Jenssen *et al.* obtained CW orange laser emission at 605 nm with 190 mW of output power and a slope efficiency of 20% employing a 2.2 at.% Sm:LiTbF$_4$ crystal (a self-activated crystal was used for boosting the pump absorption via Tb$^{3+} \rightarrow$ Sm^{3+} energy-transfer) and Ar$^+$ ion laser pumping [7]. The long luminescence lifetime of the $^4G_{5/2}$ Sm^{3+} state, and the four-level laser scheme for both orange and red transitions lead to low observed laser thresholds.

Recently, Marzahl *et al.* employed blue 2ω-OPSL at 479 nm for pumping 1.2 at.% Sm:LiLuF$_4$ and 6.8 at.% Sm:SrAl$_{12}$O$_{19}$ crystals [8]. In the former case, the red laser generated 93 mW at 648 nm with a slope efficiency of 15%. For the aluminate crystal, yet another laser transition was exploited, $^4G_{5/2} \rightarrow {}^6H_{11/2}$, falling into the deep-red spectral range (703 nm).

Sm^{3+} exhibits a self-quenching behavior due to several cross-relaxation (CR) processes, $^4G_{5/2} + {}^6H_{5/2} \rightarrow {}^6F_{11/2} + {}^6F_{7/2}$, $^4G_{5/2} + {}^6H_{5/2} \rightarrow {}^6F_{9/2} + {}^6F_{9/2}$ and $^4G_{5/2} + {}^6H_{5/2} \rightarrow {}^6F_{7/2} + {}^6F_{11/2}$, thus limiting the available doping level. Due to the large energy-gap from the metastable level to the next lower-lying one (~7400 cm^{-1}), the non-radiative path from the $^4G_{5/2}$ manifold is weak even for high-phonon energy oxide matrices. As the energetic position of the excited configuration of the opposite parity 4f^{4}5d^1 is relatively high for Sm^{3+}, excited-state absorption (ESA) into these levels will not impose a problem being typical for Pr^{3+}, an active ion commonly used to generate visible (red) emission [9]. However, due to the complex energy-level structure of Sm^{3+}, one cannot exclude the risk of 4f – 4f ESA transitions at the laser wavelengths.

Divalent samarium ions (Sm^{2+}) are also known. They enabled the first demonstration of laser action using rare-earth ions: a deep-red laser emission at 708.2 nm (the four-level $^5D_0 \rightarrow {}^7F_1$ transition) was obtained in 1961 from a 0.1 at.% Sm^{2+}:CaF$_2$ crystal at liquid He temperature under Xe flash lamp pumping [10]. Deep-red laser action in Sm^{2+}-doped SrF$_2$ and BaMgF$_4$ crystals was also demonstrated [11,12].

Monoclinic potassium rare-earth double tungstates KRE(WO$_4$)$_2$ (with RE standing for Y, Gd or Lu) are well-known laser host crystals for doping with trivalent rare-earth ions leading to laser emission in the near-IR [13]. They feature a single substitution rare-earth site and high available doping levels (up to stoichiometric compositions for certain ions), high absorption and emission cross-sections for the dopant ions in polarized light, weak luminescence quenching due to the large RE^{3+} - RE^{3+} ion separation and nearly athermal behavior. Recently, efficient deep-red (703 nm) laser action was demonstrated for a laser-pumped self-activated KEu(WO$_4$)$_2$ crystal [14]. Yellow (573 nm) and red (664 nm) lasing from a Xe flash lamp pumped Dy^{3+}-doped KY(WO$_4$)$_2$ was also reported [15].

In the present work, we report on the first red laser operation of a Sm^{3+}-doped monoclinic double tungstate $KGd(WO_4)_2$ crystal.

Single-crystals of Sm:$KGd(WO_4)_2$ were grown using the Top Seeded Solution Growth method (from the flux) using potassium ditungstate ($K_2W_2O_7$) as a solvent [13]. The starting reagents were K_2CO_3, WO_3, Gd_2O_3 and Sm_2O_3 (4N purity) taken according to the solute : solvent mass ratio of 1:5. The growth started at 1228 K. A [010]-oriented seed from undoped $KGd(WO_4)_2$ was used. The doping levels were 0.4 at.% and 0.8 at.% Sm^{3+}. The as-grown crystal was transparent and colorless, Fig. 1(a). It exhibited bright orange emission under UV lamp illumination, Fig. 1(b). Sm:$KGd(WO_4)_2$ crystallizes in the monoclinic class (sp. gr. C^6_{2h} – $C2/c$) and it is optically biaxial. The orientation of the optical indicatrix frame {N_p, N_m, N_g} is the following: the N_p-axis is parallel to the ***b***-axis and the other two axes are lying in the ***a-c*** plane. The angle N_g ^ ***c*** = 19.2°, measured outside of the monoclinic angle β = ***a*** ^ ***c*** = 130.8° [16]. Sm^{3+} ions are replacing the host-forming Gd^{3+} ones in a single type of sites (C_2 symmetry, VIII-fold oxygen coordination). The choice of $KGd(WO_4)_2$ as a host matrix is determined by the closeness of the ionic radii of Gd^{3+} (1.053 Å) and Sm^{3+} (1.079 Å).

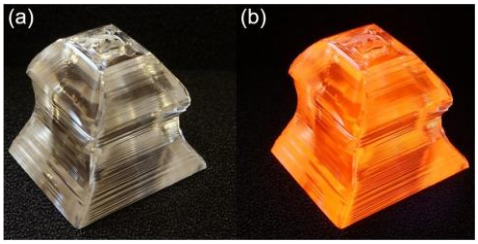

Fig. 1. A photograph of an as-grown 0.4 at.% Sm:$KGd(WO_4)_2$ crystal (the growth direction is along the [010] axis): (a) Natural light; (b) Under UV illumination.

The polarized spectroscopic properties of Sm^{3+} ions were first studied. The energy-level scheme of Sm^{3+} is depicted in Fig. 2(a). The polarized absorption cross-sections, σ_{abs}, in the blue are given in Fig. 2(b). The maximum σ_{abs} is 7.57×10^{-21} cm^2 at 478.8 nm with an absorption bandwidth (full width at half maximum, FWHM) of 2.7 nm for light polarization ***E*** || N_m. This absorption peak corresponds to the $^6H_{5/2} \rightarrow {}^4M_{15/2}$ spin-forbidden ($\Delta S \neq 0$) transition. It is well addressed by the emission of 2ω-OPSLs. At shorter wavelengths, less intense absorption peaks due to the $^6H_{5/2} \rightarrow {}^4I_{13/2}$ transition can be addressed by blue 465 nm GaN laser diodes.

The stimulated-emission (SE) cross-sections, σ_{SE}, were calculated using the Füchtbauer-Ladenburg equation based on the measured polarized luminescence spectra. The radiative lifetime of the $^4G_{5/2}$ state (τ_{rad} = 734 μs) and the luminescence branching ratio for the $^4G_{5/2} \rightarrow {}^6H_{9/2}$ transition in the red ($\beta_{J'}$ = 40.2%) were calculated using a modified Judd-Ofelt theory (mJ-O, intensity parameters: Ω_2 = 8.027, Ω_4 = 7.210, Ω_6 = 2.322 [10^{-20} cm^2] and α = -0.017 [10^{-4} cm]). The σ_{SE} are shown in Fig. 2(c). They exhibit a strong polarization anisotropy, so that linearly polarized laser emission is expected. The maximum σ_{SE} is 5.59×10^{-21} cm^2 at 649.0 nm corresponding to an emission bandwidth (FWHM) of 1.35 nm (for polarization ***E*** || N_p). For polarization ***E*** || N_m, σ_{SE} is lower, 4.54×10^{-21} cm^2 at 650.9 nm.

The luminescence decay curves from the $^4G_{5/2}$ state of Sm^{3+} ions in $KGd(WO_4)_2$ were measured, Fig. 2(d). For 0.4 at.% Sm^{3+} doping, the luminescence decay is nearly single-exponential in agreement with a single type of sites for the dopant ions (C_2 symmetry), and the average luminescence lifetime $\langle\tau_{lum}\rangle$ is 719 μs in agreement with the radiative one calculated using the mJ-O theory. Despite the high phonon energy of $KGd(WO_4)_2$ ($h\nu_{ph}$ = 901 cm^{-1}), according to the energy gap law ($\Delta E/h\nu_{ph} > 7$, where ΔE is the energy gap between the emitting state $^4G_{5/2}$ and the next lower-lying state, ~7400 cm^{-1}), the non-radiative relaxation is almost negligible.

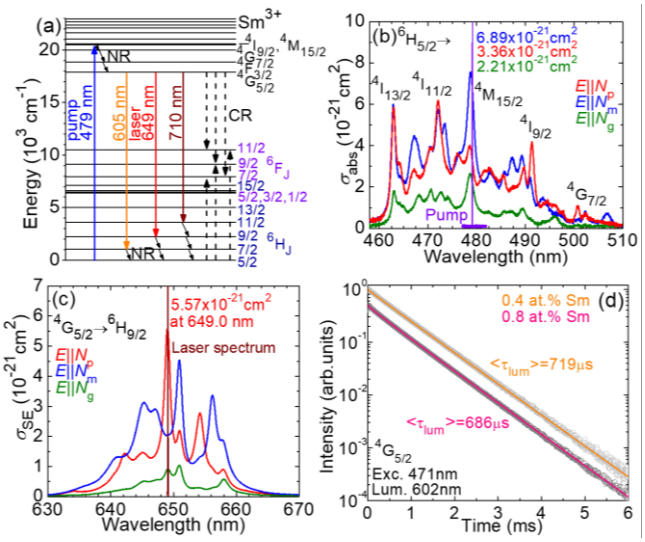

Fig. 2. Spectroscopy of Sm^{3+} ions in monoclinic $KGd(WO_4)_2$ crystal: (a) Energy-level scheme of Sm^{3+} ions, CR – cross-relaxation; (b) Polarized absorption cross-sections, σ_{abs}, at 460 – 510 nm, *violet curve* – the 2ω-OPSL spectrum; (c) Polarized SE cross-sections, σ_{SE}, for the $^4G_{5/2} \rightarrow {}^6H_{9/2}$ transition (light polarizations: ***E*** || N_p, N_m and N_g); (d) Luminescence decay curves from the $^4G_{5/2}$ state (0.4 and 0.8 at.% Sm^{3+} doping), *circles* – experimental data, *curves* – their fit using the I-H model.

On increasing the doping level to 0.8 at.%, the decay curve is no longer single-exponential due to the energy transfer between Sm^{3+} ions. It is well fitted using the Inokuti-Hirayama (I-H) model for multipolar interactions, yielding the best-fit parameters τ_0 = 750±10 μs (the intrinsic lifetime), R_0 = 7.0±0.5 Å (the critical distance for energy transfer), and s = 6 (the parameter for dipole-dipole interaction) [17]. The critical distance is smaller than the average distance between Sm^{3+} ions, R_{av} = 16.9 Å, indicating a weak effect of cross-relaxation processes, $^4G_{5/2} + {}^6H_{5/2} \rightarrow {}^6F_J + {}^6F_{J'}$, Fig. 2(a), between adjacent Sm^{3+} ions. The average luminescence lifetime for the 0.8 at.% Sm^{3+}-doped crystal $\langle\tau_{lum}\rangle$ is 686 μs.

The layout of the laser set-up is depicted in Fig. 3(a). The laser element was cut from the 0.8 at.% Sm:$KGd(WO_4)_2$ crystal (ion density: $N_{Sm} = 4.91\times10^{19}$ at/cm^3, crystal density: ρ = 7.11 g/cm^3) for light propagation along the N_g optical indicatrix axis (N_g-cut) having a thickness of 8.05 mm and an aperture of 6.00(N_p) × 7.70(N_m) mm^2, Fig. 3(b). Both its $N_p \times N_m$ faces were polished to laser-grade quality with good parallelism and left uncoated. The laser element was mounted on a passively cooled Cu-holder using a silver paint for better heat removal. The plano-concave cavity was composed of a flat pump mirror (PM) providing high transmission (T = 90.2%) at the pump wavelength of 479 nm, and high reflection (R > 99.5%) at 570 – 670 nm, and a set of concave (radius of curvature: –50 mm) output couplers (OCs) with a transmission T_{OC} of 0.1%, 0.3% and 3.0% at the laser wavelength (649 nm). The

crystal was placed near the PM with an airgap of ~1 mm. The cavity length was 45 mm. The pump source was a 2ω-OPSL (Genesis CX STM, Coherent) emitting up to 1.5 W at 479.1 nm (laser linewidth: <0.1 nm) in the fundamental mode ($M^2 \approx 1$) with a linear polarization. This wavelength allowed pumping into the $^4M_{15/2}$ Sm^{3+} state, as shown in Fig. 2(b). The polarization of the pump radiation could be adjusted by an AR-coated half-wave plate. The pump was focused into the crystal through the PM by an achromatic lens (focal length: f = 75 mm) and the average pump spot radius was 44 μm (at the $1/e^2$ level). The pumping was in single pass. The radius of the laser mode was calculated using the ABCD method to be 55 μm. A long-pass filter (FEL600, Thorlabs) was placed after the OC. The laser spectrum was measured using an optical spectrum analyzer (OSA, AQ6373B, Yokogawa) with a resolution of 0.02 nm, and the beam profile was captured with a CCD-camera (BladeCam2-XHR, DataRay). The temporal behavior of the laser output was studied using a high-speed Si photodetector (DET210, Thorlabs, rise time: 1 ns) and a 200 MHz digital oscilloscope (TDS2022B, Tektronix).

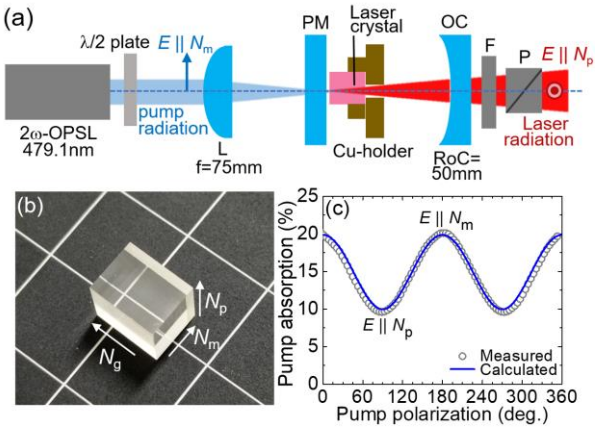

Fig. 3. Red Sm:KGd$(WO_4)_2$ laser: (a) Scheme of the laser set-up, L – AR-coated achromatic focusing lens, PM – pump mirror, OC – output coupler, F – cut-off filter, P – Glan-Taylor polarizer; (b) A photograph of a polished 0.8 at.% Sm^{3+}-doped laser element; (c) The measured pump absorption as a function of orientation of the pump polarization (with respect to the N_m-axis), *points* – experimental data, *curve* – calculation based on the polarized absorption spectra and Malus law.

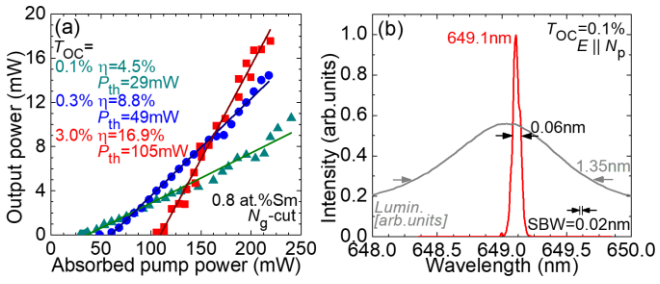

Fig. 4. (a) Input-output dependences, η – slope efficiency, P_{th} – laser threshold; (b) A typical spectrum of laser emission, T_{OC} = 0.1%, *grey curve* – fluorescence spectrum. The laser polarization is $\boldsymbol{E} \parallel N_p$.

For the studied range of pump powers, the absorption saturation was nearly negligible. The pump absorption efficiency (accounting for the Fresnel loss at the uncoated crystal faces) was measured as a function of pump polarization, Fig. 3(c). It was maximum for the polarization $\boldsymbol{E} \parallel N_m$, namely η_{abs} = 20.1%, and minimum for $\boldsymbol{E} \parallel N_p$, in agreement with the polarization anisotropy of σ_{abs} spectra for Sm^{3+} ions, see Fig. 2(b).

The effect of the output coupling on the laser performance was studied, see Fig. 4(a). The Sm-laser generated a maximum output power of 17.6 mW at 649.1 nm, with a slope efficiency η of 16.9% and a laser threshold of 105 mW (for T_{OC} = 3.0%). This result was obtained for an incident power of 1.1 W, so the corresponding optical-to-optical efficiency η_{opt} was 1.6%. On decreasing the output coupling from 3.0% to 0.1%, the laser threshold decreased to 29 mW. Such a low laser threshold is related to the four-level laser scheme of the $^4G_{5/2} \rightarrow {}^6H_{9/2}$ transition and a relatively long lifetime of the upper laser level.

The typical spectrum of laser emission for T_{OC} = 0.1% is shown in Fig. 4(b) and compared with the fluorescence spectrum. The laser wavelength, 649.1 nm (according to the $^4G_{5/2} \rightarrow {}^6H_{9/2}$ Sm^{3+} transition), was weakly dependent on the output coupling. The laser linewidth (FWHM) was 0.06 nm, compared with the emission bandwidth of 1.35 nm for the same light polarization.

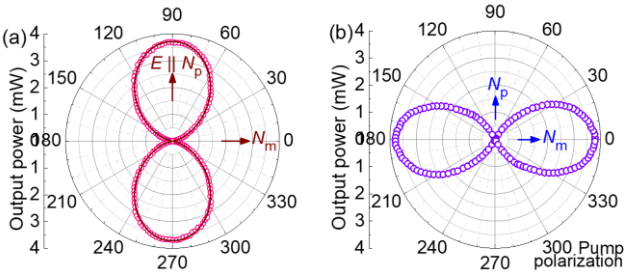

Fig. 5. Polarization behavior of red Sm:KGd$(WO_4)_2$ laser: (a) Analysis of the polarization state of laser emission; (b) Output power of the laser as a function of the pump polarization. T_{OC} = 0.1%, P_{inc} = 0.59 W.

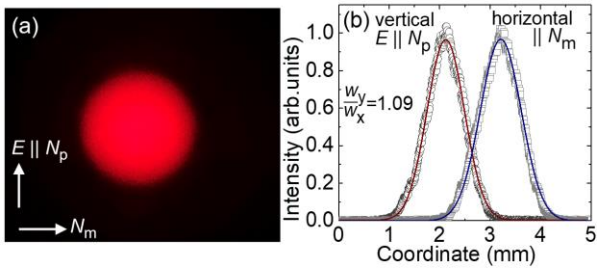

Fig. 6. Spatial characteristics of red emission from the Sm:KGd$(WO_4)_2$ laser: (a) A photograph of the laser beam in the far-field; (b) 1D intensity profiles (*symbols* – experimental data, *curves* – Gaussian fits). T_{OC} = 0.1%.

The laser emission was linearly polarized and the polarization $\boldsymbol{E} \parallel N_p$ was naturally selected by the anisotropy of the gain, Fig. 2(c). The polarization state of red laser emission was characterized using a Glan-Taylor polarizer placed after the OC. The experimental points were fitted with the formula $P(\theta) = P_u/2 + P_p\cos^2(\theta - 90°)$, where P_p / P_u is the polarized / unpolarized power fraction and θ is the angle between the polarizer axis and the N_m-axis (horizontal), Fig. 5(a). The polarization degree $P = P_p/(P_p + P_u)$ was >99.9%.

The pump polarization ($\boldsymbol{E}_p$) was then varied using a half-wave plate placed before the focusing lens, Fig. 5(b). The incident pump power was fixed to P_{inc} = 0.59 W. The red laser output was maximized when pumping into N_m polarization, and no lasing was observed for the orthogonal one $\boldsymbol{E}_p \,||\, N_p$, in agreement with the anisotropy of absorption for the $^6H_{5/2} \rightarrow {}^4M_{15/2}$ transition, Fig. 2(b). The laser threshold for pumping into $\boldsymbol{E}_p \,||\, N_p$ can be reached for higher pump levels.

A photograph of the red laser beam on a black screen in the far-field is shown in Fig. 6(a). The 1D intensity profiles along the horizontal ($x \,||\, N_m$) and vertical ($y \,||\, N_p$, the polarization direction) directions are given in Fig. 6(b). They are well fitted with a Gaussian profile. A slight beam ellipticity, w_y/w_x = 1.09, is due to the weak astigmatism of positive thermal lens in the N_g-cut laser crystal. The measured beam quality factor M^2_{xy} was below 1.15.

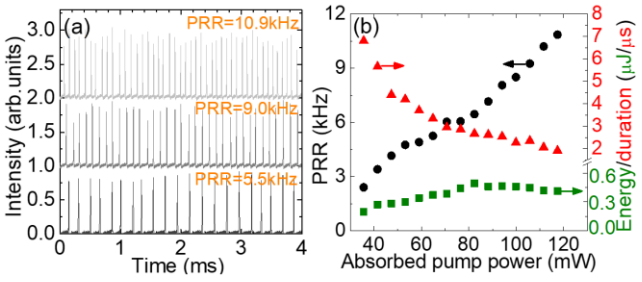

Fig. 7. Temporal dynamics of red Sm:KGd(WO$_4$)$_2$ laser: (a) Typical oscilloscope traces revealing the self-pulsed operation regime of the Sm-laser; (b) Pulse repetition rate (PRR), pulse energy / pulse duration vs. the absorbed pump power. T_{OC} = 0.1%.

The temporal dynamics of the Sm-laser was studied revealing a self-pulsing behavior. The laser generated stable trains of pulses, Fig. 7(a). The pulse characteristics were strongly dependent on the pump level. For example, for T_{OC} = 0.1%, on increasing the absorbed pump power from 35 to 117 mW, the pulse energy first increased and then saturated around 0.4 μJ, the pulse duration monotonously dropped from 3.7 to 1.91 μs (being much shorter than the upper laser level, $^4G_{5/2}$, lifetime, Fig. 2(d)), and the pulse repetition rate (PRR) gradually increased from 2.4 to 10.9 kHz, Fig. 7(b). The self-pulsing behavior has been observed previously for other Sm lasers based on both fluoride and oxide crystals. This behavior resembles passive Q-switching by a "fast" saturable absorber (SA). Excited-state absorption (ESA) from the $^4G_{5/2}$ metastable manifold at the laser wavelength can serve as such an artificial SA. According to our analysis, around 650 nm, there are non-resonant ESA transitions to the short-living $^4P_{5/2}$ (E = 32620 cm^{-1}) and $^2F_{5/2}$ (33510 cm^{-1}) states with noticeable transition intensities. Direct ESA measurements are required to clarify this issue.

We also tried to achieve laser operation on the $^4G_{5/2} \rightarrow {}^6H_{7/2}$ Sm^{3+} transition (in the orange) using spectrally selective mirrors, but the laser threshold was not reached. We also predict a strong resonant ESA around 600 nm, related to transitions to the $^4F_{9/2}$, $^2L_{17/2}$ and $^4I_{9/2}$ states (34240 – 34430 cm^{-1}).

To conclude, Sm^{3+}-doped KGd(WO$_4$)$_2$ double tungstate crystal is a suitable gain medium for laser sources directly emitting in the red spectral range. It is because of high absorption cross-sections in the blue for polarized light despite the spin-forbidden ($\Delta S \neq 0$) nature of the corresponding transitions, a long luminescence lifetime of the upper laser level and high stimulated-emission cross-sections in the red (five times those for Sm^{3+}:LiLuF$_4$). In the present work, for a 0.8 at.% Sm:KGd(WO$_4$)$_2$ laser operating on the $^4G_{5/2} \rightarrow {}^6H_{9/2}$ transition (at 649.1 nm), a slope efficiency up to 16.9% and a laser threshold as low as 29 mW were obtained. We also observed an interesting self-pulsing operation regime with generation of μs-long pulses at high repetition rates (kHz-range), and assigned this behavior to non-resonant 4f – 4f ESA to the short-living $^4P_{5/2}$ and $^2F_{5/2}$ states acting as an artificial "fast" saturable absorber. Further power scaling is envisioned by increasing the Sm^{3+} doping level (to balance the pump absorption efficiency and self-quenching by CR), using longer samples as well as employing diode-pumping. Direct ESA spectral measurements in the orange, red and deep-red spectral ranges are required to understand the limitations for laser emission in Sm:KGd(WO$_4$)$_2$ at these wavelengths. Another open question is the interaction of Gd^{3+} and Sm^{3+} ions, namely, the Gd^{3+}(^6P_J) → Sm^{3+}(^4P_J) energy transfer.

Funding. Agence Nationale de la Recherche (ANR-22-CE08-0025-01, NOVELA); Contrat de plan État-Région (CPER) de Normandie.

Disclosures. The authors declare no conflicts of interest.

Data availability. Data underlying the results presented in this paper are not publicly available at this time but may be obtained from the authors upon reasonable request.

References

1. C. Kränkel, D.-T. Marzahl, F. Moglia, G. Huber, and P. W. Metz, Laser Photon. Rev. **10**, 548 (2016).
2. J. Li, J. Yan, D. Wen, W. U. Khan, J. Shi, M. Wu, Q. Su, and P. A. Tanner, J. Mater. Chem. C **4**, 8611 (2016).
3. L. Walsh, Aust. Dent. J. **48**, 146 (2003).
4. W. Denk, J. H. Strickler, and W. W. Webb, Science **248**, 73 (1990).
5. B. N. Kazakov, M. S. Orolov, M. V. Petrov, A. L. Stolov, and A. M. Tkachuk, Opt. Spectrosc. **47**, 676 (1979).
6. M. C. Farries, P. R. Morkel, and J. E. Townsend, "Electron. Lett. **24**, 709 (1988).
7. H. P. Jenssen, in *Advanced Solid-State Lasers* (ASSL Technical Digest, 1995), paper ME2-1/73.
8. D.-T. Marzahl, P. W. Metz, C. Kränkel, and G. Huber, Opt. Express **23**, 21118 (2015).
9. P. Dorenbos, J. Condens. Matter Phys. **15**, 8417 (2003).
10. P. P. Sorokin, and M. J. Stevenson, IBM J. Res. Dev. **5**, 56 (1961).
11. P. P. Sorokin, M. J. Stevenson, J. R. Lankard, and G. D. Pettit, Phys. Rev. **127**, 503 (1962).
12. H. H. Zenzie, T. M. Pollak, E. P. Chicklis, and K. L. Schepler, in *Advanced Solid State Lasers*, vol. 20 OSA Technical Digest (Optica Publishing Group, 1987), paper TuD18.
13. V. Petrov, M. Cinta Pujol, X. Mateos, O. Silvestre, S. Rivier, M. Aguilo, R. M. Sole, J. Liu, U. Griebner, and F. Diaz, Laser Photonics Rev. **1**, 179 (2007).
14. P. Loiko, D. Rytz, S. Schwung, P. Pues, T. Jüstel, J.-L. Doualan, and P. Camy, Opt. Lett. **46**, 2702 (2021).
15. A. Kaminskii, U. Hömmerich, D. Temple, J. T. Seo, K.-I. Ueda, S. Bagayev, and A. Pavlyuk, Jpn. J. Appl. Phys. **39**, L208 (2000).
16. P. Loiko, P. Segonds, P.L. Inácio, A. Peña, J. Debray, D. Rytz, V. Filippov, K. Yumashev, M.C. Pujol, X. Mateos, M. Aguiló, F. Díaz, M. Eichhorn, and B. Boulanger, Opt. Mater. Express **6**, 2984-2990 (2016).
17. M. Inokuti and F. Hirayama, J. Chem. Phys. **43**, 1978 (1965).

Full references

1. C. Kränkel, D.-T. Marzahl, F. Moglia, G. Huber, and P. W. Metz, "Out of the blue: semiconductor laser pumped visible rare-earth doped lasers," Laser Photon. Rev. **10**(4), 548-568 (2016).
2. J. Li, J. Yan, D. Wen, W. U. Khan, J. Shi, M. Wu, Q. Su, and P. A. Tanner, "Advanced red phosphors for white light-emitting diodes," J. Mater. Chem. C **4**(37), 8611-8623 (2016).
3. L. Walsh, "The current status of laser applications in dentistry," Aust. Dent. J. **48**(3), 146-155 (2003).
4. W. Denk, J. H. Strickler, and W. W. Webb, "Two-photon laser scanning fluorescence microscopy," Science **248**(4951), 73-76 (1990).
5. B. N. Kazakov, M. S. Orolov, M. V. Petrov, A. L. Stolov, and A. M. Tkachuk, "Induced emission of Sm^{3+} ions in the visible region of the spectrum," Opt. Spectrosc. **47**, 676–677 (1979).
6. M. C. Farries, P. R. Morkel, and J. E. Townsend, "Samarium^{3+}-doped glass laser operating at 651nm", Electron. Lett. **24**(11), 709-711 (1988).
7. H. P. Jenssen, "Visible (orange) laser emission from Sm-doped $LiTbF_4$," in *Advanced Solid-State Lasers* (ASSL Technical Digest, 1995), paper ME2-1/73.
8. D.-T. Marzahl, P. W. Metz, C. Kränkel, and G. Huber, "Spectroscopy and laser operation of Sm^{3+}-doped lithium lutetium tetrafluoride ($LiLuF_4$) and strontium hexaaluminate ($SrAl_{12}O_{19}$)," Opt. Express **23**(16), 21118-21127 (2015).
9. P. Dorenbos, "Systematic behaviour in trivalent lanthanide charge transfer energies," J. Condens. Matter Phys. **15**(49), 8417 (2003).
10. P. P. Sorokin, and M. J. Stevenson, "Solid-state optical maser using divalent samarium in calcium fluoride," IBM J. Res. Dev. **5**(1), 56-58 (1961).
11. P. P. Sorokin, M. J. Stevenson, J. R. Lankard, and G. D. Pettit, "Spectroscopy and optical maser action in SrF_2:Sm^{2+}," Phys. Rev. **127**(2), 503 (1962).
12. H. H. Zenzie, T. M. Pollak, E. P. Chicklis, and K. L. Schepler, "Laser emission at 679.8 nm in Sm^{2+}:$BaMgF_4$," in *Advanced Solid State Lasers*, vol. 20 OSA Technical Digest (Optica Publishing Group, 1987), paper TuD18.
13. V. Petrov, M. Cinta Pujol, X. Mateos, O. Silvestre, S. Rivier, M. Aguilo, R. M. Sole, J. Liu, U. Griebner, and F. Diaz, "Growth and properties of $KLu(WO_4)_2$, and novel ytterbium and thulium lasers based on this monoclinic crystalline host," Laser Photonics Rev. **1**(2), 179-212 (2007).
14. P. Loiko, D. Rytz, S. Schwung, P. Pues, T. Jüstel, J.-L. Doualan, and P. Camy, "Watt-level europium laser at 703 nm," Opt. Lett. **46**(11), 2702-2705 (2021).
15. A. Kaminskii, U. Hömmerich, D. Temple, J. T. Seo, K.-I. Ueda, S. Bagayev, and A. Pavlyuk, "Visible laser action of Dy^{3+} Ions in monoclinic $KY(WO_4)_2$ and $KGd(WO_4)_2$ crystals under Xe-flashlamp pumping," Jpn. J. Appl. Phys. **39**(3A), L208-L211 (2000).
16. P. Loiko, P. Segonds, P.L. Inácio, A. Peña, J. Debray, D. Rytz, V. Filippov, K. Yumashev, M.C. Pujol, X. Mateos, M. Aguiló, F. Díaz, M. Eichhorn, and B. Boulanger, "Refined orientation of the optical axes as a function of wavelength in three monoclinic double tungstate crystals $KRE(WO_4)_2$ (RE = Gd, Y or Lu)," Opt. Mater. Express **6**(9), 2984-2990 (2016).
17. M. Inokuti and F. Hirayama, "Influence of energy transfer by the exchange mechanism on donor luminescence," J. Chem. Phys. **43**(6), 1978-1989 (1965).